1978

Finite Element Analysis of Fluid Flow Using Variational Approach

W. W. Hallam

FINITE ELEMENT ANALYSIS OF FLUID FLOW USING VARIATIONAL APPROACH

W.W. Hallam, B.Sc., Senior Engineer,
Sperry Gyroscope, Bracknell, Berks.

SYNOPSIS

This paper describes the Finite Element method, using variational principles to enable steady state forces on and around a disc valve to be determined.

Both two-dimensional and axisymmetric flow cases can be considered for either confined or free surface boundary problems.

An axisymmetric confined boundary problem using steady-state (static) flow conditions is described in this paper (potential flow). Comparison is then drawn between this method and previously obtained experimental data (2,3) which for completeness also includes dynamic forces as well as the steady-state forces.

The agreement was found to be good over the range considered.

1. INTRODUCTION

The behaviour of fluids as they issue from various 'orifice type' profiles can be of great interest to engineers in obtaining discharge and contraction coefficients and since much work has been carried out on these types of problems (1), the next stage would appear to be in obtaining a general technique to enable velocity, pressure and hence force profiles to be obtained for various boundaries and flow conditions. This would hopefully result in more realistic values for the above parameters and would then contribute to the possible alleviation of expensive and time consuming experimental methods by varying the relevant parameters in the above theoretical package.

One such type of problem is considered and it is hoped that the main underlying principles involved in obtaining a general solution are fully clarified. Also the problem chosen is concerned with conditions relevant to those obtained in a compressor, i.e. flow leaving an orifice and passing around a valve(2).

2. EXPERIMENTAL BACKGROUND

Previous experimental work has already been presented at Purdue (3), these results being used as a basis of comparison for the theoretical analysis subsequently outlined in this paper.

The experimental static results were obtained using the rig as shown in FIGURE 1 and during these static tests, measurements were taken by setting the various parameters - pressure, displacement etc., to their respective dynamic values. When steady conditions had been obtained, the gas flow was interrupted and the drop in force recorded on the oscilloscope. A typical family of curves obtained from these tests is shown in FIGURE 2 and the cross curve derived is shown in FIGURE 3. This curve exhibits a minimum value which is typical of all such cross curves over the entire range of measurement.

This rig was also used for the dynamic tests, where initially the plenum chamber was pressurised with the valve closed. Upon opening of the valve to the required displacement, simultaneous readings of pressure, force and displacement were recorded on the oscilloscope. Subsequently static and dynamic experimental results were compared, FIGURES 4 and 5. It will be seen that during the early part of the valve opening process there is a significant difference between the dynamic force and the quasi-static force. This is more marked when there is a high pressure difference across the valve. Also when the valve is opened relatively slowly, the dynamic force curve conforms more closely to the quasi-static force curve.

3. THEORETICAL ANALYSIS

In this section the fundamental theory on which the mathematical model is based will be presented. The example chosen is based on axisymmetric potential fluid flow theory and uses the Finite Element method for a confined boundary case. The method employs the velocity potential $\emptyset$ as the primary unknown and 8-node quadrilateral elements of arbitrary shape to

represent the region of flow under study. This method is equally applicable to more complex flow conditions and to both confined and free-surface flow problems. The method first computes a solution for the velocity potential throughout the entire flow domain and then calculates secondary unknowns such as velocity, pressure and force distributions. A general flow domain is shown in FIGURE 6.

(1) Problem Formulation for Axisymmetric Flow

Both a velocity potential ϕ and a stream function ψ exist to aid the present study of a steady, axisymmetric, irrotational flow of an ideal fluid. However, formulation in terms of the velocity potential function appears to be much simpler, because it bears a close resemblance to the formulation for two-dimensional flows.

In variational form the velocity potential problem to be solved is that of minimising the function:

$$I(\phi) = \rho\pi \iint_A [(\phi_{,x})^2 + (\phi_{,r})^2]\, r\,dr\,dx - 2\rho\pi \oint_C \phi\,(\phi_{,n})^a\, r\,ds \quad \text{(Equ. (1))}$$

The first term on the right hand side is the kinetic energy in the entire flow region, and the second term, with the integration carried out on the portion of surface boundary where the normal velocity component is specified, represents twice the work done by the impulsive force in starting the flow to move from rest. This equation resembles the one for two-dimensional flow (Equ. (2)) except that in place of y, the radius r has been used.

$$I(\phi) = \frac{\rho}{2} \iint_A [(\phi_{,x})^2 + (\phi_{,y})^2]\, dx\,dy - \rho \oint_C \phi\,(\phi_{,n})^a\, ds \quad \text{(Equ. (2))}$$

The minimisation of $I(\phi)$ is equivalent to solving the Laplace equation:

$$\phi_{,xx} + \frac{1}{r}\phi_{,r} + \phi_{,rr} = 0 \text{ in } A \quad \text{(Equ. (3))}$$

with $$\phi_{,n} = (\phi_{,n})^a \text{ on } C \quad \text{(Equ. (4))}$$

In the Finite Element formulation, the region to be analysed is divided into N′ subregions, (NB Each quadrilateral element is now a cross-section of an annular region through which flow occurs) or finite elements and Equ. (1) can be replaced by:

$$I(\phi) = \sum_{e=1}^{N'} I^e(\phi) \quad \text{(Equ. (5))}$$

where $$I^e(\phi) = \rho^e\pi \iint_{A^e} [(\phi^e_{,x})^2 + (\phi^e_{,r})^2]\, r\,dr\,dx - 2\rho^e\pi \oint_{C^e} \phi^e\,(\phi_{,n})^a\, r\,ds \quad \text{(Equ. (6))}$$

represent the energy of a typical element e, which may, in turn, consist of several sub-elements. A typical quadrilateral element, composed of four triangular elements is shown in Figure 7. Each triangular element has three corner nodes and three side nodes, one at the midpoint of each side. The triangular or area co-ordinates are:

$$L_i = A_i / A^{(m)} \quad \text{(Equ. (7))}$$

where $A^{(m)}$ = area of entire triangle

and A_i = area of one subtriangle

Thus the side connecting nodes 1 and 2 is described by

$L_3 = 0$ and also $L_1 + L_2 + L_3 = 1$.

For the conditions in each triangular element, $\phi^{(m)}$ is approximated by a second order polynomial of the form:

$$\phi^{(m)} = \phi_i^{(m)} \cdot Ni^{(m)} \quad (i = 1 \text{ to } 6) \quad \text{(Equ. (8))}$$

where

$$N_i = [L_1(2L_1 - 1), L_2(2L_2 - 1), L_3(2L_3 - 1), 4L_1L_2, 4L_2L_3, 4L_3L_1] \quad \text{(Equ. (9))}$$

The velocity components are:

$$V_x = \frac{\partial \phi}{\partial x} \quad \text{and} \quad V_r = \frac{\partial \phi}{\partial r} \quad \text{(Equ. (10))}$$

become

$$V_x^{(m)} = \phi_{,x}^{(m)} = \phi_i^{(m)} \cdot T_i^{(m)} \quad (i = 1 \text{ to } 6) \quad \text{(Equ. (11))}$$

and $$V_r^{(m)} = \phi_{,r}^{(m)} = \phi_i^{(m)} \hat{T}_i^{(m)} \quad (i = 1 \text{ to } 6) \quad \text{(Equ. (12))}$$

with $$T_i^{(m)} = (4L_i - 1)b_i / 2A^{(m)} \quad \text{(Equ. (13))}$$
(no summation on i)

and $$T_{(i+3)}^{(m)} = 4(b_i L_j + b_j L_i)/2A^{(m)} \quad \text{(Equ. (14))}$$
(no summation on i)

where $a_k = x_j - x_i$, $b_k = r_i - r_j$, (Equ. (15))

$$2A^{(m)} = a_k b_j - a_j b_k$$

$$i = (1,2,3),\ j = (2,3,1),\ k = (3,1,2) \quad \text{(Equ. (16))}$$

The array $\hat{T}_i^{(m)}$ is found by replacing the b's with a's in the expression for $Ti^{(m)}$. In addition to the above equations, the variable r is introduced as:

$$r = r_1 L_1 + r_2 L_2 + r_3 L_3 \quad \text{(Equ. (17))}$$

where r_1, r_2 and r_3 are radial co-ordinates of the corner nodes 1, 2 and 3 respectively, and L_1, L_2 and L_3 are again the area co-ordinates of a point in a triangular element. Upon substituting equations (8), (11), (12), (13) and (14) into equation (6) (Note: subscript (m) must be used in place of e to designate calculations for a triangular element) followed by computing the partial derivatives of $I^{(m)}$ ϕ. with respect to $\phi^{(m)}$ and interchanging subscripts i and j one obtains

$$\frac{\partial I^{(m)}(\phi)}{\partial \phi_i^{(m)}} = 2\rho^{(m)}\pi \iint_{A^{(m)}} \left(T_i^{(m)} T_j^{(m)}\right) + \left(\hat{T}_i^{(m)} \hat{T}_j^{(m)}\right) r \phi_j^{(m)} dA - 2\rho^{(m)} \oint_{C^{(m)}} N_i(\phi, n)^a r\, ds \qquad \text{(Equ.(18))}$$

$$\text{or } \frac{\partial I^{(m)}(\phi)}{\partial \phi_i^{(m)}} = SA_{ij}^{(m)} \phi_j^{(m)} - SLA_i^{(m)} \qquad \text{(Equ.(19))}$$

$$0 = [SA]^{(m)} \{\phi\}^{(m)} + \{SLA\}^{(m)} \qquad \text{(Equ.(20))}$$

Now the necessary minimizing condition is that the left hand side = 0, and it will also be noticed that in Equ. (20) the last term is +ve, this is dependent on the convention used for the defining of the direction of the boundary velocity. In the terms of structural mechanics $SAij^{(m)}$ and $SLA_i^{(m)}$ are the element stiffness and load matrices respectively which are listed in section (9) of this report.

The contribution from each triangle in a quadrilateral element is first evaluated, followed by appropriately adding up all the contributions to the 13 nodal points. The equations for the 5 interior points of the quadrilateral are then eliminated at the element level to obtain the element stiffness matrix $SAij^e$ and its load matrix SLA_i^e for a quadrilateral element. The expressions for each quadrilateral are then added together appropriately to form the system matrices, which is identical to the direct stiffness method of structural mechanics.

The resulting system of equations is linear, symmetric and in band form. The total number of equations is equal to the total number of nodal points, and the bandwidth is equal to one plus the difference between the largest and smallest node number in a quadrilateral element.

This system of equations is then solved for the ϕ_i's by Gaussian elimination. Once the ϕ_i's are known, the velocity components at any point can be calculated and likewise the pressure and force distributions.

4. THEORETICAL PROCEDURE

The flow domain was as shown in FIGURE 8. Various grid arrangements were chosen to enable X and Y to be minimised for a specific valve displacement 'h'.

The upstream pressure is set equal to the experimental pressure at the corresponding displacement, and subsequently the upstream velocity is calculated from equation 21.

The computed theoretical static forces are shown in FIGURES 4 and 5.

5. COMMENTS

The difference between the theoretical and experimental steady state forces appear to have good agreement throughout the range covered but because of the 'small' difference between the experimental dynamic and static results full agreement is difficult to interpret. It is believed that this method could satisfactorily meet the requirements in determining forces on and around a disc valve and could be extended to cover the large and varied problems encountered in the field. Further work is continuing at this time.

6. ACKNOWLEDGEMENTS

This work was originally carried out at the University of Strathclyde in the Dynamics and Control Department and latterly at Sperry Gyroscope, Bracknell.

7. REFERENCES

1. Chan S.T.K. Fluid Flows from axisymmetric orifices and valves. Proc. A.S.C.E. Hydraulics division Jan. 1973 pp 81-97.

2. Hallam, W.W. Thesis (to be published).

3. Brown, J., Davidson, R., Hallam, W.W. Dynamic Measurement of Valve Lift Force. Purdue Compressor Technology Conference 1976.

8. NOMENCLATURE

$A^{(m)}$	= area of triangle
A_1	= upstream area
A_2	= downstream area
C	= portion of line boundary on which normal velocity components are specified
e	= a subscript used to indicate calculation for a quadrilateral element e

h	= valve opening (lift)
$I(\phi)$	= functional of velocity potential ϕ
$I^e(\phi)$	= functional for quadrilateral element e
i,j,k	= subscripts used to designate points i,j,k
m	= superscript used to indicate calculation for triangular element m
N	= total number of finite elements
n,s	= natural co-ordinates, i.e. outward normal direction and tangential direction, respectively
p	= pressure
P_1	= pressure upstream
q	= speed or magnitude of velocity
qd	= downstream asymptotic speed
qu	= upstream speed
r	= radial co-ordinate
SA_{ij}^e	= element matrix for element e
SLA_i^e	= load matrix for element e
$Ti, {}^{(m)}, \hat{Ti}^{(m)}$	= arrays expressing geometric properties of triangular element m
Vr, Vx	= Velocity components in radial and axial directions respectively
x,y	= rectangular cartesian co-ordinates
L_1, L_2, L_3	= area co-ordinates of point in triangle
ρ	= fluid density
ϕ	= velocity potential function
$(\phi_{,n})^a$	= specified normal velocity component
$\phi, {}_x\phi, {}_y\phi$ etc.	= partial derivative of function designation
π	= 3.142
a_i	= algebraic difference of two points in x direction
bi	= algebraic difference of two points in r direction

9. APPENDIX

Element Stiffness and Load Matrices for Axi-symmetric Flow.

if $$S_{ij} = \frac{(a_i a_j + b_i b_j)\rho^{(m)}}{60A^{(m)}}$$

then

$$SA_{11}^{(m)} = 3S_{11}(3r_1+r_2+r_3)$$

$$SA_{12}^{(m)} = SA_{21}^{(m)} = -S_{12}(2r_1+2r_2+r_3)$$

$$SA_{13}^{(m)} = SA_{31}^{(m)} = -S_{13}(2r_1+r_2+2r_3)$$

$$SA_{14}^{(m)} = SA_{41}^{(m)} = S_{11}(3r_1-2r_2-r_3) + S_{12}(14r_1+3r_2+3r_3)$$

$$SA_{15}^{(m)} = SA_{51}^{(m)} = S_{12}(3r_1-r_2-2r_3) + S_{13}(3r_1-2r_2-r_3)$$

$$SA_{16}^{(m)} = SA_{61}^{(m)} = S_{11}(3r_1-r_2-2r_3) + S_{13}(14r_1+3r_2+3r_3)$$

$$SA_{22}^{(m)} = 3S_{22}(r_1+3r_2+r_3)$$

$$SA_{23}^{(m)} = SA_{32}^{(m)} = -S_{23}(r_1+2r_2+2r_3)$$

$$SA_{24}^{(m)} = SA_{42}^{(m)} = S_{12}(3r_1-14r_2+3r_3) + S_{22}(-2r_1+3r_2-r_3)$$

$$SA_{25}^{(m)} = SA_{52}^{(m)} = S_{22}(-r_1+3r_2-2r_3) + S_{23}(3r_1+14r_2+3r_3)$$

$$SA_{26}^{(m)} = SA_{62}^{(m)} = S_{12}(-r_1+3r_2-2r_3) + S_{23}(-2r_1+3r_2-r_3)$$

$$SA_{33}^{(m)} = 3S_{33}(r_1+r_2+3r_3)$$

$$SA_{34}^{(m)} = SA_{43}^{(m)} = S_{13}(-r_1-2r_2+3r_3) + S_{23}(-2r_1-r_2+3r_3)$$

$$SA_{35}^{(m)} = SA_{53}^{(m)} = S_{23}(3r_1+3r_2+14r_3) + S_{33}(-r_1-2r_2+3r_3)$$

$$SA_{36}^{(m)} = SA_{63}^{(m)} = S_{13}(3r_1+3r_2+14r_3) + S_{33}(-2r_1-r_2+3r_3)$$

$$SA_{44}^{(m)} = 8\left[S_{11}(r_1 + 3r_2 + r_3) + S_{12}(2r_1 + 2r_2 + r_3) + S_{22}(3r_1+r_2+r_3)\right]$$

$$SA_{45}^{(m)} = SA_{54}^{(m)} = 8S_{13}(r_1 + 3r_2 + r_3) - 4(S_{12}r_1+S_{22}r_2+S_{23}r_3)$$

$$SA_{46}^{(m)} = SA_{64}^{(m)} = 8S_{23}(3r_1+r_2+r_3) + 4(S_{11}r_1+S_{12}r_2+S_{13}r_3)$$

$$SA_{55}^{(m)} = 8\left[S_{22}(r_1 + r_2 + 3r_3) + S_{23}(r_1 + 2r_2 + 2r_3) + S_{33}(r_1+3r_2+r_3)\right]$$

$$SA_{56}^{(m)} = SA_{65}^{(m)} = 8S_{12}(r_1 + r_2 + 3r_3) - 4(S_{13}r_1 + S_{23}r_2 + S_{33}r_3)$$

$$SA_{66}^{(m)} = 8\left[S_{11}(r_1 + r_2 + 3r_3) + S_{13}(2r_1 + r_2 + 2r_3) + S_{33}(3r_1+r_2+r_3)\right]$$

In the load matrix terms, l_i = length of side i of a triangular sub-element. Thus:

$$SAL_1^{(m)} = r_1\left[(\emptyset,n)^{a2} l_2 + (\emptyset,n)^{a3} l_3\right] \frac{\rho^{(m)}}{6}$$

$$SAL_2^{(m)} = r_2\left[(\emptyset,n)^{a1} l_1 + (\emptyset,n)^{a3} l_3\right] \frac{\rho^{(m)}}{6}$$

$$SAL_3^{(m)} = r_3\left[(\emptyset,n)^{a1} l_1 + (\emptyset,n)^{a2} l_2\right] \frac{\rho^{(m)}}{6}$$

$$SAL_4^{(m)} = (r_1 + r_2)(\emptyset,n)^{a3} l_3 \frac{\rho^{(m)}}{3}$$

$$SAL_5^{(m)} = (r_2 + r_3)(\emptyset,n)^{a1} l_1 \frac{\rho^{(m)}}{3}$$

$$SAL_6^{(m)} = (r_3 + r_1)(\emptyset,n)^{a2} l_2 \frac{\rho^{(m)}}{3}$$

EXPERIMENTAL TEST RIG.

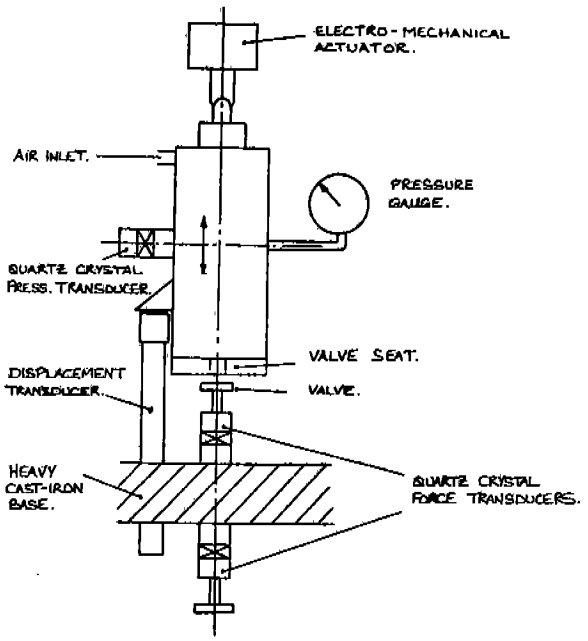

FIGURE 1.

STEADY-FLOW TEST RESULTS.

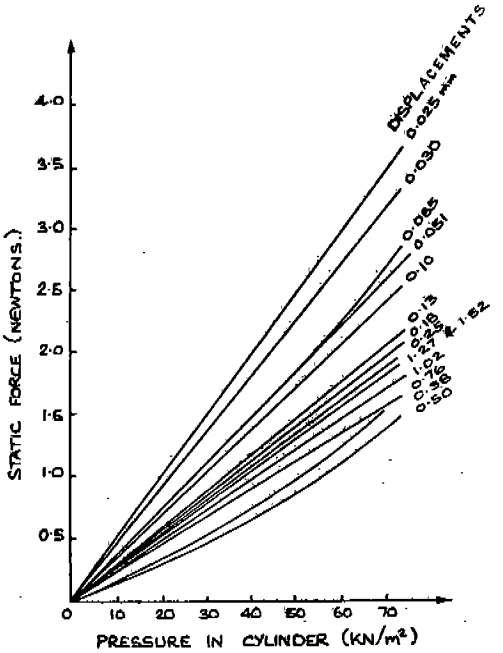

FIGURE 2.

DERIVED CURVE FROM STEADY-FLOW RESULTS.

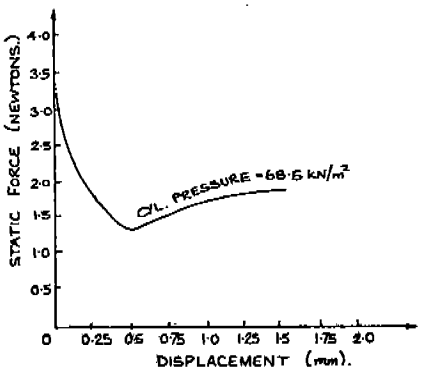

VALVE DISC. 9·50 mm O.D.
PORT. 6·35 mm BORE.

FIGURE 3.

COMPARISON OF CALCULATED STATIC FORCES WITH EXPERIMENTAL DYNAMIC & STATIC FORCES.

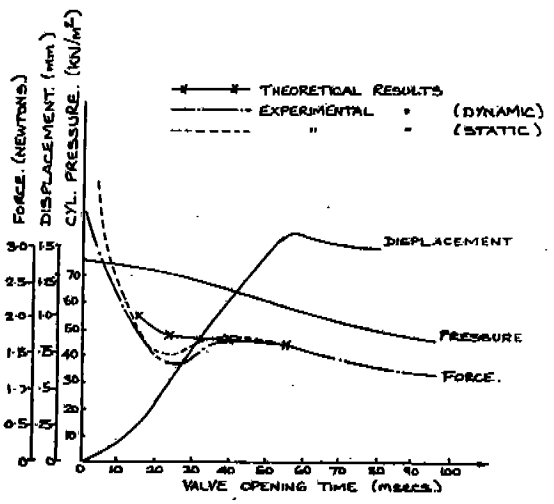

VALVE DISC. 9·50 mm O/D.
PORT. 6·35 mm BORE.
CYL. PRESSURE. 77 kN/m².

FIGURE 4.

COMPARISON OF CALCULATED STATIC FORCES WITH EXPERIMENTAL DYNAMIC & STATIC FORCES.

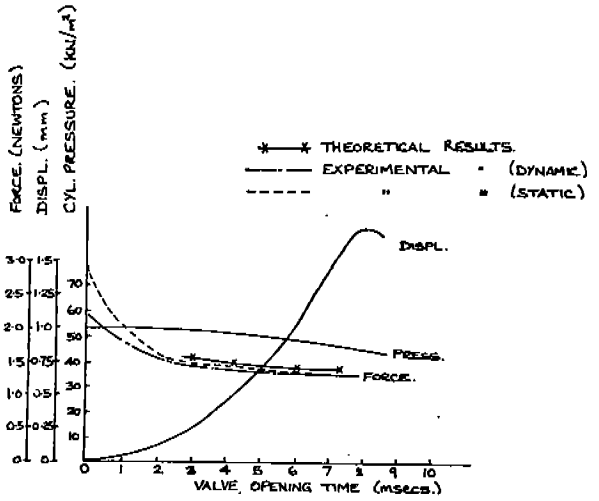

VALVE DISC. 8·40 mm OD.
PORT. 6·35 mm BORE.
CYLINDER PRESSURE 54 kN/m².

FIGURE 5.

GENERAL FLOW DOMAIN.

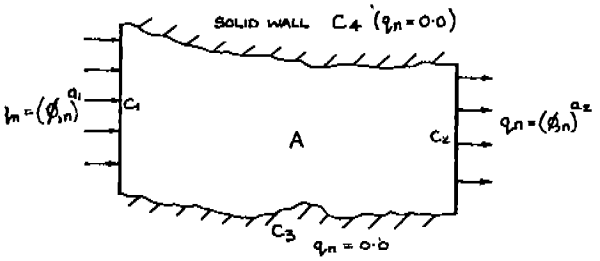

$$C = C_1 + C_2$$

$$B = C_1 + C_2 + C_3 + C_4$$

FIGURE 6.

QUADRILATERAL ELEMENT & ITS SUBELEMENT.

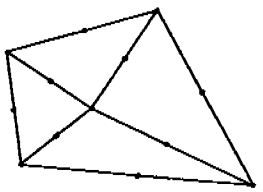

a) QUADRILATERAL ELEMENT.

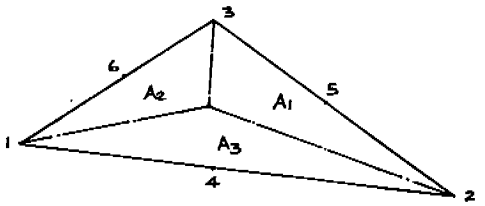

b) TRIANGULAR SUBELEMENT. (2D.)

FIGURE 7.

THEORETICAL FLOW DOMAIN.

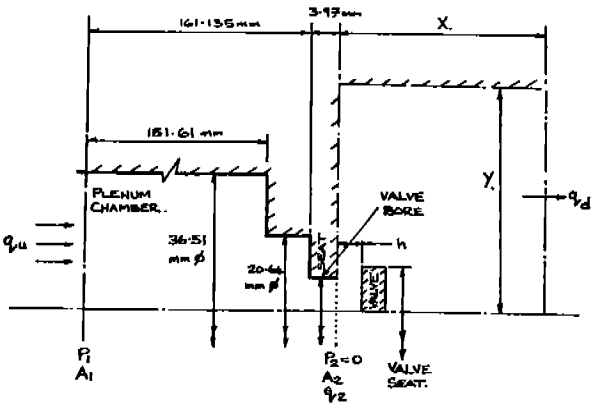

$$q_u = \sqrt{\frac{2P_1}{\rho}\left(\frac{A_2^2}{A_1^2 - A_2^2}\right)} \qquad \text{EQU. 21.}$$

$$q_2 A_2 = q_u A_1 \qquad \text{EQU. 22.}$$

FIGURE 8. (N.T.S.)